

University of Groningen

Ultrahigh Mobility in an Organic Semiconductor by Vertical Chain Alignment

Skrypnychuk, Vasyli; Wetzelaer, Gert-Jan A. H.; Gordiichuk, Pavlo I.; Mannsfeld, Stefan C B; Herrmann, Andreas; Toney, Michael F.; Barbero, David R.

Published in:
Advanced materials

DOI:
[10.1002/adma.201503422](https://doi.org/10.1002/adma.201503422)

IMPORTANT NOTE: You are advised to consult the publisher's version (publisher's PDF) if you wish to cite from it. Please check the document version below.

Document Version
Publisher's PDF, also known as Version of record

Publication date:
2016

[Link to publication in University of Groningen/UMCG research database](#)

Citation for published version (APA):

Skrypnychuk, V., Wetzelaer, G-J. A. H., Gordiichuk, P. I., Mannsfeld, S. C. B., Herrmann, A., Toney, M. F., & Barbero, D. R. (2016). Ultrahigh Mobility in an Organic Semiconductor by Vertical Chain Alignment. *Advanced materials*, 28, 2359-2366. <https://doi.org/10.1002/adma.201503422>

Copyright

Other than for strictly personal use, it is not permitted to download or to forward/distribute the text or part of it without the consent of the author(s) and/or copyright holder(s), unless the work is under an open content license (like Creative Commons).

The publication may also be distributed here under the terms of Article 25fa of the Dutch Copyright Act, indicated by the "Taverne" license. More information can be found on the University of Groningen website: <https://www.rug.nl/library/open-access/self-archiving-pure/taverne-amendment>.

Take-down policy

If you believe that this document breaches copyright please contact us providing details, and we will remove access to the work immediately and investigate your claim.

Downloaded from the University of Groningen/UMCG research database (Pure): <http://www.rug.nl/research/portal>. For technical reasons the number of authors shown on this cover page is limited to 10 maximum.

Ultrahigh Mobility in an Organic Semiconductor by Vertical Chain Alignment

Vasyl Skrypnichuk, Gert-Jan A. H. Wetzelaer, Pavlo I. Gordiichuk, Stefan C. B. Mannsfeld, Andreas Herrmann, Michael F. Toney, and David R. Barbero*

Conjugated polymers with high mobilities are paramount for developing more efficient organic electronic devices such as organic field-effect transistors (OFETs), organic photovoltaics (OPVs), and organic light-emitting diodes (OLEDs). Polythiophene polymers, e.g., poly(3-hexylthiophene) (P3HT), have been among the most studied materials for OPVs due to their strong optical absorbance and ease of processing from solution. However, the out-of-plane (vertical) charge carrier mobility of P3HT, which is required for fast charge transport in OPVs and OLEDs, is typically much too low ($\approx 0.001 \text{ cm}^2 \text{ V}^{-1} \text{ s}^{-1}$) for producing efficient devices. Here, we demonstrate highly efficient long range out-of-plane charge transport in P3HT reaching record high average mobilities above $3.1 \text{ cm}^2 \text{ V}^{-1} \text{ s}^{-1}$. This large enhancement in charge transport is achieved by controlled orientation of the polymer crystallites enabling the most efficient and fastest charge transport along the chain backbones and across multiple chains. These results open up the route to producing high mobility conjugated polymer films without chemical modification of the polymer, and they may also help better design more efficient electronic devices with vertical charge transport, e.g., OLEDs and OPVs.

Conjugated, or conducting, polymers possess the unique ability to absorb light, create charges, and transport them in a bulk heterojunction solar cell.^[1–3] Moreover, due to their ease of processing into a thin solid film from solution, conducting polymers have long promised to enable the production of low-cost

and high performance printed electronics and flexible photovoltaic solar cells.^[4] Due to its excellent optoelectronic properties, regio-regular P3HT (rr-P3HT; **Figure 1a**) has been one of the most studied conducting polymers for plastic electronics.^[5–10] However, its relatively low charge-carrier mobility compared to silicon and other inorganic materials^[11] has limited its potential for use in commercial applications.

Charge transport in conjugated polymers occurs either in the direction of π - π stacking, through interchain electronic orbital overlap, or along the chain backbone which is the fastest transport direction inside a crystalline aggregate. Terahertz experiments have shown that high mobility can be achieved on very short distances, along the chain backbone, in undoped P3HT.^[12] However, the mobility quickly drops as charges must hop from one crystalline domain to another in order to be transported over larger distances. Structural disorder, defects and poor interconnectivity have been shown to trap charges and reduce mobility in conjugated polymers.^[13]

Enhanced crystallinity and charge-carrier mobility in P3HT have previously been achieved by temperature annealing,^[14–18] increased degree of regio-regularity,^[19] or higher molecular weight.^[20] However, mobility strongly depends on the orientation of crystalline domains, which also influence the direction of charge transport. In the horizontal OFET configuration, charges are transported in the plane of the film, with crystalline lamellae mainly parallel to the substrate (edge-on, **Figure 1b**). However, some applications (OPVs,^[21–23] OLEDs,^[24–27] vertical OFETs^[28–31]) require charge transport in the vertical direction (normal to the plane of the film). For these, vertical orientation of either the π stacking (face-on), or of the chain backbone (chain-on, **Figure 1b**), the latter being the fastest charge transport route, is needed to efficiently direct charges in the out-of-plane direction. Partial vertical alignment of P3HT chains has been reported in silicon nanogrooves infiltrated with a P3HT:PCBM blend,^[32] and in P3HT infiltrated into alumina nanopores.^[33,34] The highest vertical (out-of-plane) charge-carrier mobility reported to date in P3HT is $6 \times 10^{-3} \text{ cm}^2 \text{ V}^{-1} \text{ s}^{-1}$.^[33] By comparison, in-plane OFET mobilities of $0.2\text{--}0.4 \text{ cm}^2 \text{ V}^{-1} \text{ s}^{-1}$ have been reported in P3HT.^[35,36] Previous work has shown partial vertical alignment in nanogratings (nanoscale lines), which was assigned to hydrophobic interactions between a silicon mold coated with 1H,1H,2H,2H-per-fluorodecyltrichlorosilane (FDTS) molecules and the hexyl side chains of P3HT.^[21,37] However, charge transport in the vertical direction was not measured, and no conclusion was drawn between vertical chain alignment and mobility in the vertical direction.^[37] In organic optoelectronic devices, an efficient and balanced charge transport in the vertical direction helps

V. Skrypnichuk, Prof. D. R. Barbero
Nano-Engineered Materials & Organic Electronics
Laboratory
Umeå University
Umeå 90187, Sweden
E-mail: david.barbero@umu.se
Dr. G.-J. A. H. Wetzelaer,^[†] P. I. Gordiichuk,
Prof. A. Herrmann
Polymer Chemistry and Bioengineering
Zernike Institute for Advanced Materials
University of Groningen
Nijenborgh 4 9747 AG, Groningen, The Netherlands
Prof. S. C. B. Mannsfeld,^[††] Dr. M. F. Toney
Materials Science Division
Stanford Synchrotron Radiation Lightsource
Menlo Park, CA 94025, USA



[†] Present address: Polymer Research, Max Planck Institute, Mainz 55128, Germany.

[††] Present address: Center for Advancing Electronics, Technische Universität Dresden, Dresden 01887, Germany.

DOI: 10.1002/adma.201503422

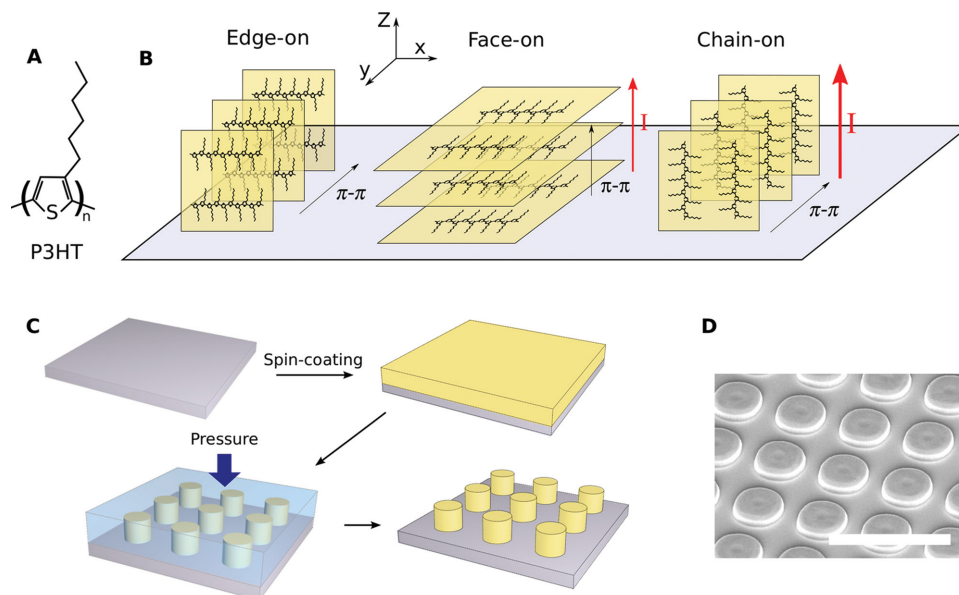


Figure 1. Chain orientation in rr-P3HT crystallites, and sample patterning. a) Chemical structure of P3HT. b) From left to right: Edge-on lamellae with π - π stacking in the plane of the film; face-on lamellae with π - π stacking perpendicular to the plane of the film; chain-on orientation with the P3HT chain backbone vertically oriented along the z axis, which enables more efficient vertical charge transport. c) The film is spun from solution onto a substrate, and imprinted with a PDMS mold to form micropatterns in the rr-P3HT film. d) SEM image of the resulting micropatterns in P3HT. Scale bar in (d) is 10 μm .

reduce recombination, and achieve higher efficiency (e.g., OPVs) and higher brightness (e.g., OLEDs). However the low mobility of most organic semiconductors has been a major hurdle to increase device performance. In order to increase the efficiency of organic electronic devices that require vertical charge transport, and make them competitive with other non-organic technologies, higher charge-carrier mobilities in the vertical direction must be achieved. Moreover, the ability to experimentally direct charges along the fastest transport route (chain backbone) on relatively long distances (10s to 100s of chain lengths) is of high fundamental importance because previously high mobilities above $10\text{ cm}^2\text{ V}^{-1}\text{ s}^{-1}$ ^[12] had only been observed in highly ordered domains and on very short distances in P3HT.

In this letter, we demonstrate 3 orders of magnitude enhancement in out-of-plane charge-carrier mobility in an undoped P3HT film.^[33,34] A combination of nanoscale electrical measurements, synchrotron X-ray diffraction and polarized microscopy revealed that these unprecedented high mobilities are due to charge transport along the vertically reoriented polymer chains and crystallites (chain-on), enabled by the vertical nanoscale flow of the viscous polymer during nanopatterning. These mobilities rival that of inorganic materials,^[38] and may open up the possibility to produce more efficient organic electronic devices with vertical charge transport. Moreover, vertical chain alignment by this method is very versatile due to the possibility to change the processing parameters (pressure, temperature, time, mold's material, etc) over a large range of experimental conditions, and to optimize these for a specific polymer, structure, and application.

As shown in Figure 1c, the thin films were prepared by spin-coating a dilute solution of rr-P3HT (rr: 98%, $M_w = 32\,000\text{ g mol}^{-1}$) onto a silicon substrate, and nanoimprinting

of the film with a flexible poly-dimethylsiloxane (PDMS) mold at a temperature of 200 $^{\circ}\text{C}$ for 5 min.^[39–41] The film was then cooled down to room temperature at which point the mold was removed. This process produced an array of periodic and well defined micropatterns (Figure 1d) with dimensions identical to that of the mold (diameter $\approx 4\text{ }\mu\text{m}$; periodicity $\approx 6\text{ }\mu\text{m}$; height $\approx 1\text{ }\mu\text{m}$). For reference, a smooth rr-P3HT film was also prepared by spinning and annealing/cooling in the same conditions in inert atmosphere. Nanoimprinting is a powerful method which has been used to form well defined micro- and nanoscale domains in polymers, and which has resulted in improved electrical properties in polymer nonvolatile memories,^[42] and in solar cells.^[23] The charge-carrier mobility of micropatterned P3HT has, however, never been measured in the vertical (diode) direction. Previously, nanopatterning of P3HT has resulted in improved crystallinity and partial vertical chain orientation in line nanogratings (width 65 nm, periodicity 200 nm), but the vertical charge transport was not investigated in those structures and no correlation between chain alignment and vertical mobility was proposed.^[21,37] Moreover, it is important to realize that confinement effects due to size (nano vs micro) and shape (line vs dot) can greatly influence both crystalline orientation and electrical properties. Therefore, one cannot simply assume that a particular chain alignment measured, e.g., in a nanostructure (either lines grating or dots), will result in the same chain orientation and crystallinity as in a micropillar. For the same reason, the electrical properties of these two different geometries and sizes will most likely be different. Moreover, the flow of the material under pressure, as well as the timescale under which this occurs, are important parameters which will determine crystalline orientation, and mobility in a given type of structure. Processing conditions

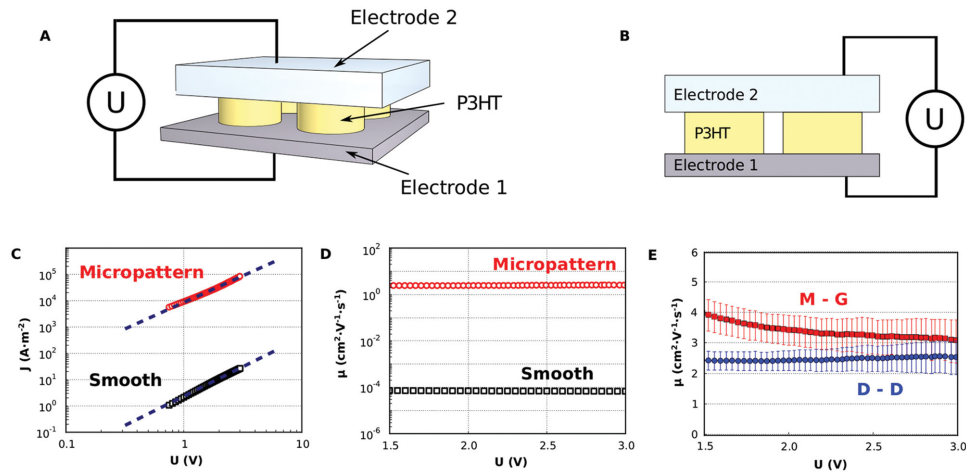


Figure 2. Macroscopic electrical properties of the *rr*-P3HT films. a) 3D schematics of the macroscopic measurement, where a potential difference U is applied between the conductive substrate and an electrode lying on top of the film, and the current flowing vertically through the film is measured. b) Cross-section view of the schematics of the macroscopic measurement. c) Log-Log plots of macroscopic vertical current density J in a smooth film, and in a micropatterned film, showing space-charge limited transport in both samples (slope ≈ 2.0). d) Vertical charge-carrier mobility in a smooth, and in a micropatterned film (log scale). e) Vertical charge-carrier mobility in a micropatterned film by both Mott-Gurney and drift-diffusion models (linear scale).

(temperature, pressure, time, etc.) therefore need to be optimized for each polymer and structure to obtain the desired result. It is therefore of great importance to investigate the crystallinity and electrical properties of various sizes and shapes of patterns in the diode (vertical) configuration.

The vertical current flow perpendicular to the film's surface was measured by two different and complementary methods. In the first method, a potential difference was applied between the flat top surface of the P3HT patterns and the conductive silicon substrate (resistivity $\approx 0.002\text{--}0.005\ \Omega\ \text{cm}$; electrode 1, Figure 2a,b), and the resulting macroscopic current density was measured across the film thickness by dividing the current by the total surface area at the top of the pillars. Good conformal contact between the top electrode (electrode 2, Figure 2a,b) and the top of the pillars was ensured by the use of a semiflexible electrode made of an elastomeric/Ag composite material (see the Supporting Information for experimental details). Characterization by electron microscopy confirmed that the electrode made good contact with the top of the micropillars and did not bend nor directly contact the thin residual layer in between the pillars (see Figure S1, Supporting Information), eliminating the possibility of creating an electrical short. Redoing the same J - V electrical measurement with insulating polystyrene micropatterns resulted in negligible background currents (10 orders of magnitude lower than in the P3HT micropatterns) thereby proving that no leakage current was present during the measurements (see the Supporting Information) and that the two electrodes did not contact each other.

As shown in Figure 2c the current density across the patterned film was about 4–5 orders of magnitude higher than in the smooth unpatterned film at the same bias. The macroscopic mobilities (shown in Figure 2d,e) were extracted by fitting the J - V characteristics with: (1) the classical drift-only description of the space-charge-limited current by Mott and Gurney (M-G), see Equation (1); (2) an analytical drift-diffusion (D-D) model (see Equation (2)),^[43,44] which improves the analysis

with respect to the classical drift-only equation at low voltages.^[45] The equations of mobility, derived for a planar metal–semiconductor–metal junction,^[44] are

$$\text{Mott-Gurney: } J = \frac{9}{8} \epsilon \mu \frac{U^2}{L^3} \quad (1)$$

$$\text{Drift-Diffusion: } J = \epsilon \mu \frac{U}{L^3} \left(4\pi^2 \frac{kT}{q} + \frac{9}{8} U \right) \quad (2)$$

with μ the charge-carrier mobility, J the current density, L the film thickness, ϵ the permittivity, U the voltage, k the Boltzmann constant, T the temperature, and q the elementary charge. Average macroscopic out-of-plane mobilities of $\approx 3.1 \pm 0.7\ \text{cm}^2\ \text{V}^{-1}\ \text{s}^{-1}$ and $\approx 2.6 \pm 0.6\ \text{cm}^2\ \text{V}^{-1}\ \text{s}^{-1}$ were measured in air in the micropatterned sample using the M-G and the D-D models respectively, and are summarized in Table 1. By comparison, mobilities of $\approx 10^{-4} \pm 0.4 \times 10^{-4}\ \text{cm}^2\ \text{V}^{-1}\ \text{s}^{-1}$ were measured in a smooth film spun and annealed in the same conditions. In both samples the current exhibited a quadratic voltage dependence (Figure 2c) at higher voltages (slope ≈ 2.0), typical for a space-charge-limited drift current and characteristic of charge transport through an intrinsic semiconductor. At lower

Table 1. Mobility values of the micropatterned P3HT film measured by macroscopic and c-AFM methods. For the macroscopic measurements, the mobility was calculated using both the classical Mott-Gurney model (M-G), and the drift-diffusion model (D-D).

Micropatterned sample	μ [$\text{cm}^2\ \text{V}^{-1}\ \text{s}^{-1}$]		
	Whole pillar	Pillar edge	Pillar center
Macroscopic mobility (D-D model)	2.6 ± 0.6	–	–
Macroscopic mobility (M-G model)	3.1 ± 0.7	–	–
c-AFM mobility	–	10.6 ± 4.6	2.3 ± 1.0

voltages, the deviation between the two models (Figure 2d,e) is due to the diffusion component of the current which is not taken into account in the M-G model. The charge transport therefore followed more accurately the D-D model at lower voltages, and the patterned film was consequently well described by a space-charge-limited current (with a diffusion and drift component) through an undoped semiconductor. Additional details of the macroscopic electrical characterization are given in the Supporting Information.

A second electrical characterization method was performed on the patterned film using a conductive atomic force microscope (c-AFM, Figure 3). Here we measured a local nanoscale current by applying a potential difference between the conductive tip of an AFM and the substrate, and measuring the current flowing through an individual pillar. This method therefore enabled a measure of the local nanoscale electrical properties of the film. The local I - V characteristics were treated with an analytical model derived for a conductive AFM experiment on an intrinsic semiconductor.^[46] The hole mobility injected from the plane was extracted from the J - V data using the following equation

$$J = \frac{3}{2} \epsilon \mu \frac{U^2}{L^3} \quad (3)$$

where the current density (J) was extracted by calculating the contact area between the AFM tip and the surface of the sample using the Johnson, Kendall, and Roberts (JKR) theory of elastic deformation (see the Supporting Information for details). As predicted by the equation, the experimentally measured current had a quadratic dependence on voltage, characteristic of a space-charge-limited current through an undoped semiconductor (see Figure S2, Supporting Information).

The c-AFM current map in Figure 3b revealed that the patterned film is composed of highly conductive 3D pillars and

of very weakly conductive smooth regions in between the pillars, which correspond to a very thin (≈ 6 – 8 nm) residual layer. The average mobility in the top central part of the pillars corresponds to $\approx 2.3 \pm 1.0 \text{ cm}^2 \text{ V}^{-1} \text{ s}^{-1}$, which is close to the mobility measured by the macroscopic method described above. Moreover, the cross-section current mapping of the micropillars (Figure 3c) shows that the edges at the top of the pillars are even more conductive than in the center, with an average mobility $\approx 10.6 \pm 4.6 \text{ cm}^2 \text{ V}^{-1} \text{ s}^{-1}$. It should be noted that although these values agree well with the macroscopic measurements of the mobility, which gives an averaged value over the whole surface at the top of the pillars (see Table 1), one should consider the order of magnitude (1 – $10 \text{ cm}^2 \text{ V}^{-1} \text{ s}^{-1}$) obtained by c-AFM as a confirmation of the high mobility measured rather than as an exact value. The reason is due to the difficulty to know precisely the contact area between the tip and the surface, which cannot be measured directly. Our calculation however assumed an upper bound of the contact area, which gave a lower value of the mobility (see the Supporting Information for details).

Polarized microscopy performed on the patterned samples showed a clear molecular anisotropy at the periphery of the pillars (Figure 3d–f), where bright rings were observed at all rotation angles, whereas other parts of the sample remained mostly dark. This indicates a vertical chain orientation at the edges of the pillars (see the Supporting Information). It is more or less well known that crystallinity and crystalline orientation strongly affects charge transport in thin conjugated films, and in order to understand the large difference in the charge-carrier mobilities between the smooth and patterned films, one must look in detail at the crystallinity and chain orientation of each film.

The crystallinity and microstructure of the patterned P3HT films were characterized by 2D synchrotron grazing incidence X-ray diffraction (2D GIXD) (BL 11-3), and by out of plane specular diffraction with a point detector (BL 2-1) at the Stanford

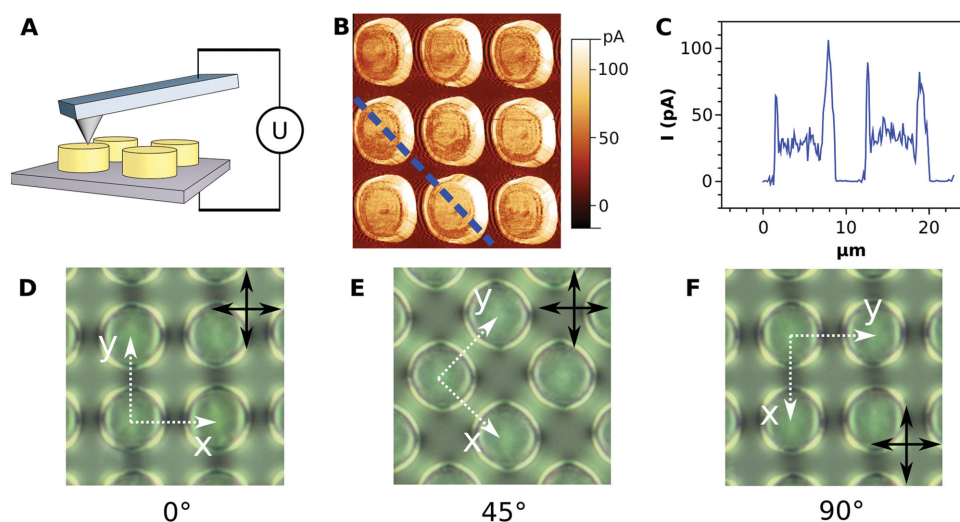


Figure 3. Nanoscale electrical properties, and polarized microscopy, of the patterned films. a) Schematic of the c-AFM measurement where a potential difference U is applied between the substrate and the conductive AFM tip. b) 2D plot of the vertical current measured in conductive AFM mode. Notice the highly conductive region in the outer part of the patterns. Dark regions are weakly conducting, bright regions are more conductive. c) Cross section of the micropillars in conductive mode (broken line in (b)) showing highly conductive regions at the periphery of the patterns, and less conductive regions in the center. d–f) Cross polarized microscopy at three different rotation angles, showing a strong anisotropy and alignment of chain backbones at the periphery of the micropillars (bright rings).

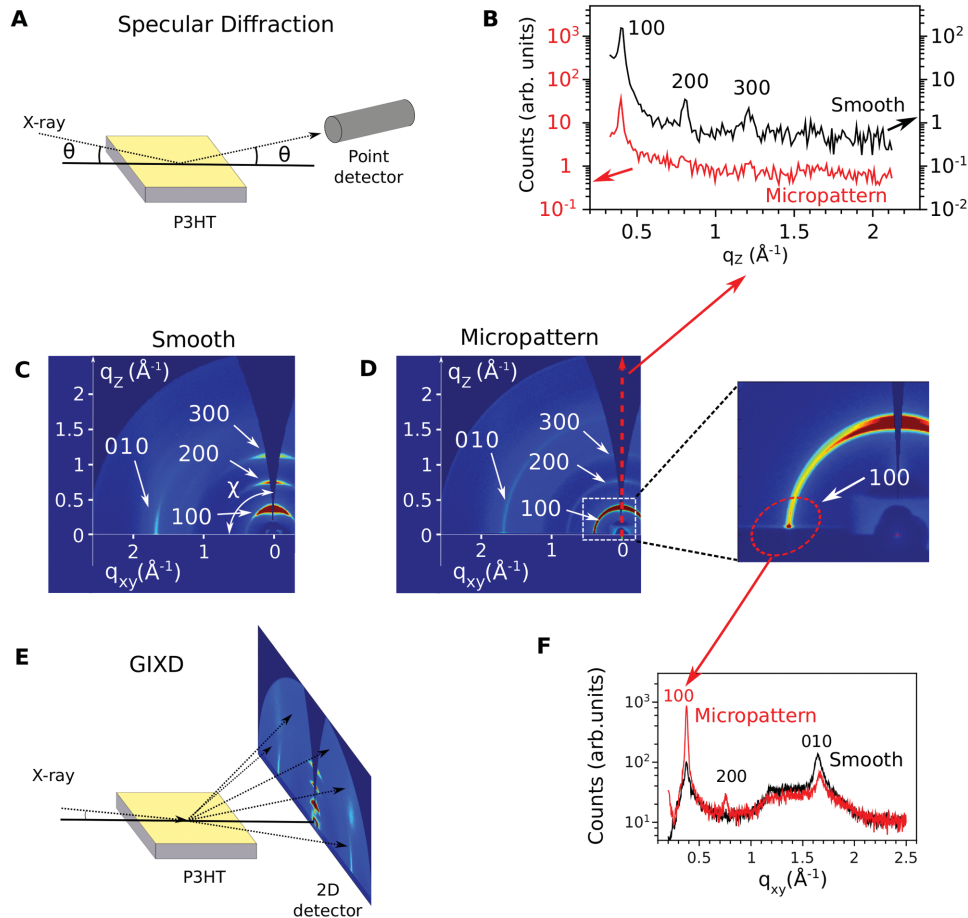


Figure 4. Crystalline structure of a smooth and a micropatterned P3HT film. a) Geometry of the specular X-ray diffraction set-up with a point detector. b) Specular diffraction of a smooth and micropatterned film, showing very weak vertical π stacking ($q_z \approx 1.65 \text{ \AA}^{-1}$) in the micropatterned film. c) 2D GIXD patterns of a smooth film, and d) of a micropatterned film showing strong in-plane (100) diffraction arcs (inset) which are only present in the micropatterned film. e) Geometry of the grazing incidence GIXD with a 2D planar detector. f) In-plane X-ray diffraction intensity cross sections for the micropatterned (red line), and the smooth (black line) films. A strong (100) peak ($q_{xy} = 0.38 \text{ \AA}^{-1}$) is clearly visible only in the micropatterned film.

National Accelerator Laboratory (SLAC, Stanford, USA). The resulting diffraction data (Figure 4) show the family of (h 00) diffraction planes near the out of plane direction (z axis) which are clearly visible in both patterned and nonpatterned films and are characteristic of edge-on lamellae. One clear difference however is the well-defined diffraction ring at (100) in the patterned sample, and the two intense arcs of intensity along the (xy) plane near $q_z = 0$, which shows the presence of crystallites with either vertical π - π stacking or vertical chain alignment in the patterned film. This is clearly seen by the intense diffraction spot in the magnified excerpt in Figure 4d, and the strong (100) peak in the micropattern in Figure 4f. By contrast, only very weak (100) diffraction along (xy) (≈ 10 times less intense) is visible in the smooth film (Figure 4f; see also Figure S4, Supporting Information). The smooth film therefore consists mainly of edge-on lamellae, which is consistent with previous reports on spun P3HT films.^[47] The diffraction patterns shown in Figure 4c–f were recorded on a planar area detector (Figure 4e), which limits slightly the polar angles accessible at large q due to the curvature of the Ewald sphere. In order to determine accurately whether the intense (100) in-plane diffraction peaks come from vertical

π - π stacking or vertical chain alignment, we also performed specular X-ray diffraction (BL 2-1) (Figure 4a,b). This method enabled an accurate estimate of the (010) diffracted intensity indicative of vertical π - π stacking. The out-of-plane diffraction data (Figure 4b) showed no (010) peak ($q_z \approx 1.65 \text{ \AA}^{-1}$) above the noise level (with counts ≈ 100 times less than the (100) peak). This means that vertical π - π stacking is very weak, if any, in the patterned films, which consist mainly of edge-on and chain-on crystallites, and of a mosaic of crystallites with their π stacking randomly oriented away from the z axis, as shown by the ring at the (100) position which extends from in-plane ($\chi = 90^\circ$) to out-of-plane angles ($\chi \approx 2^\circ$) in Figure 4d.

Typically, vertical charge transport is assumed to be along π stacking (face-on) in P3HT, however this is not the fastest charge transport route, and the highest experimentally reported mobility in highly face-on oriented P3HT films is ≈ 3 orders of magnitude lower than the mobilities measured here.^[48,49] Moreover, only a negligible amount of face-on oriented lamellae were measured in our samples (see Figure 4b), therefore ruling out the possibility that face-on lamellae could be responsible for the high mobility measured. Instead, the chain-on crystalline orientations

Table 2. Highest average mobilities reported in the literature for P3HT, and compared to the results of this study.

Measurement type	μ [$\text{cm}^2 \text{V}^{-1} \text{s}^{-1}$]	Reference
Horizontal – FET	0.2–0.4	[35,36]
Vertical – diode	0.006	[33]
Vertical – micropattern	3.1–10.6	(This work)
Terahertz spectroscopy	30–40	[12]
Theoretical calculation	31	[55]

and vertical chain alignment measured in the micropatterned sample can help us understand the high charge carrier-mobility. The difference in processing conditions between the smooth and the patterned films is critical in determining the final crystallinity and charge transport properties of each type of sample. In the smooth film, the polymer chains were mainly oriented in the plane of the film by the spin-coating process. This resulted in mainly edge-on crystallites, which conduct charges poorly in the out-of-plane direction. However, in the patterned film the P3HT chains were sheared and reoriented vertically during imprinting due to the directed nanoscale flow of the viscous melted polymer along the side walls of the mold under pressure. This is supported by the chain-on orientation observed by GIXD in the patterned sample, which is indicative of vertically aligned chains. This vertical alignment enables a fast and efficient charge transport along the chains backbone, which is the fastest transport direction inside chain-on crystalline aggregates. Long range transport is then likely provided by vertically aligned tie-chains connecting aggregates and crystallites, and results in the high mobilities measured in the vertical direction inside the patterns. We estimated that vertical charge transport occurred on a distance which represents ≈ 16 to 48 chains connected to each other in the vertical direction (see calculation in the Supporting Information).

It is useful to notice that partial chain alignment in nanostructures was previously assigned to hydrophobic interactions between a silicon mold coated with FDTS molecules and the side chains of P3HT molecules.^[21] However, in our case we used a different mold material (an elastomer PDMS), and we did not add any adsorbed molecules or coating on our molds, therefore the alignment observed likely does not have the same origin as in these works. The high hole mobility and the crystalline structure of the micropillars can instead be explained by the shearing imposed on the viscous P3HT melt along the mold's cavity during nanoimprinting^[50] which produces vertical chain alignment. The strongest shearing occurs next to the surface of the mold,^[51–54] and therefore stronger vertical chain alignment is likely to occur at the periphery of the micropatterns, as supported by the polarized microscopy data (Figure 3d–f). This resulted in a higher vertical mobility of $10.6 \text{ cm}^2 \text{V}^{-1} \text{s}^{-1}$ at the edges of the pillars as

measured by c-AFM, and is the highest ever reported mobility measured experimentally in undoped P3HT. This value comes close to the mobility estimated by density functional theory and by an acoustic deformation potential model, and also to that measured along the backbone of a chain by terahertz-probe spectroscopy.^[12,55] Values of the mobility reported in the literature by various methods are summarized in **Table 2**, and compared to our results. Even, if one considers a large error in the tip-surface contact area by c-AFM, the order of magnitude of the vertical mobility is still much higher than previously reported, and of the same order at that measured with a flat electrode. It should also be noted that terahertz spectroscopy probes only short range transport along the backbone of a chain. Our samples were however much thicker, with micropillars $\approx 1050 \text{ nm}$ high, and the charge transport was measured over relatively large distances. This means that nanoimprinting can produce ordered alignment and vertical orientation of chains over relatively large distances. The high mobility obtained here in an organic semiconductor could be beneficial for several optoelectronic applications. For example, OLEDs with microstructures have shown increased brightness compared to nanostructured ones.^[25] Therefore, microstructures with enhanced mobility could help further increase OLEDs performance thanks to faster charge transport and better charge balance.

Moreover, the flow of the polymer which is responsible for the chain alignment in the micropatterns should also result in a similar alignment in smaller nanostructures, and could also produce enhanced mobility in these. One should however notice that size effects and shearing in smaller structures may not produce the same mobility values as in micropatterns. Nanostructured organic semiconductors with high vertical mobility could help increase the hole charge transport and the charge balance in the active layer of an OPV, and help

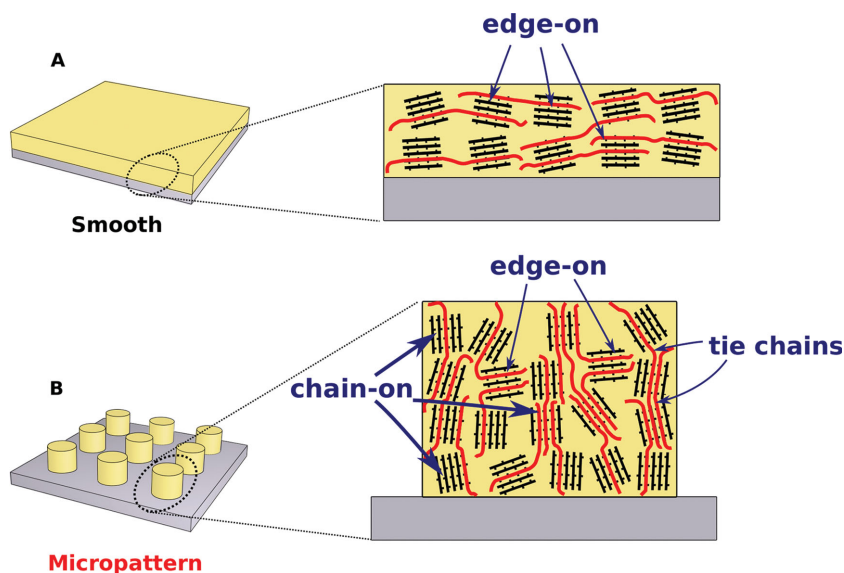


Figure 5. Schematic of possible packing arrangement of crystalline regions in a 2D smooth film and in a 3D micropatterned film. a) Edge-on lamellae with chain backbone and π stacking in the plane of the film give poor vertical charge transport in the 2D smooth film. b) A combination of chain-on and randomly oriented crystallites, with vertical chain alignment and tie-chains (red lines) connecting crystallites vertically, promote a very efficient charge transport mechanism and high hole mobility in the vertical direction inside the micropatterns.

reduce recombination. We also would like to point out that the high vertical charge-carrier mobilities measured here are in good agreement with recent reports of high in-plane mobility in a donor-acceptor copolymer which was attributed to charge transport along horizontally aligned chain backbones^[56] inside nanogrooves in a OFET configuration. Notice that no significant shearing occurred in this case, unlike in our experiments, but these results nevertheless support the fact that chain alignment, either vertical or horizontal, can produce high mobilities in organic semiconductors.

Finally, we propose in **Figure 5** the possible crystalline arrangement in both samples. In the first case (smooth planar film, **Figure 5a**), the P3HT chains form a typical edge-on lamellar structure with in-plane π stacking and chains oriented principally in the horizontal plane. In the patterned film however (**Figure 5b**), the formation of the micropillars produces an atypical composite morphology, with a mixture of edge-on, randomly oriented lamellae and chain-on crystallites which are interconnected by vertically oriented tie-chains induced by the vertical flow of polymer during imprinting. Randomly oriented and chain-on crystallites favor charge extraction in the vertical direction. The effect of vertically oriented crystallites and tie-chains is stronger at the edges of the pillars due to a stronger shear flow near the edges of the mold. In this configuration, charges can therefore be transported vertically, directly along the chain backbones of vertically aligned chains, whereas inter-chain transport can occur efficiently due to tie-chains bridging the gap between individual crystallites.^[57] This produces a very efficient charge transport from the bottom to the top of the pillars, and enables very high mobilities, without chemical modification of the polymer. The simplicity, and versatility of this method makes it highly attractive for the development of low cost thin film processed OPVs and OLEDs.

In conclusion, we have demonstrated that vertical chain orientation in P3HT produces very high mobility through fast charge transport along the chain backbones. We measured the electrical properties of such films by two different and complementary methods which revealed an unusual composite structure composed of a highly conductive region in the outer rim of the patterns, and a less conductive region in the central part of the top of the pattern. Vertical hole mobilities as high as $10.6 \text{ cm}^2 \text{ V}^{-1} \text{ s}^{-1}$ were measured by c-AFM conductivity measurements. These are the highest charge carrier mobilities ever reported in undoped P3HT, and show that high mobilities comparable to that of inorganic materials can be obtained over relatively large distances in polymers by control of the polymer chain orientation. It is expected that this work will find a wide interest among scientists working in the fields of organic electronics, polymer physics, and photovoltaics.

Experimental Section

Materials and Sample Preparation: Poly-3-hexylthiophene (P3HT) (American Dye Source, Inc) films were deposited by spin-coating from a dilute solution onto clean silicon substrates. The films were either annealed at 200 °C and slowly cooled down under inert atmosphere (smooth films), or patterned with a soft microstructured mold at the same temperature and slowly cooled down to room temperature. More details can be found in the Supporting Information.

Electrical Characterization: The vertical conductivity and mobility in the P3HT samples was calculated by measuring the current flowing between the bottom and the top of the film by two methods: macroscopic planar electrodes, and by c-AFM as explained in the text. More details can be found in the Supporting Information.

X-Ray Characterization: Grazing incidence synchrotron X-ray diffraction (GIWAXD) measurements were performed at the Stanford Synchrotron Radiation Lightsource (SSRL). All the diffraction experiments were performed in a helium-filled chamber in order to reduce background scattering and to avoid sample damage by the beam. Data analysis was performed with WxDiff software. More details can be found in the Supporting Information.

Supporting Information

Supporting Information is available from the Wiley Online Library or from the author.

Acknowledgements

Portions of this research were carried out at the Stanford Synchrotron Radiation Lightsource, a Directorate of SLAC National Accelerator Laboratory and an Office of Science User Facility operated for the U.S. Department of Energy Office of Science by Stanford University. The authors thank the Baltic Foundation and the Kempe Foundation for financial support. V.S. acknowledges support from a Kempe Scholarship. D.R.B. thanks a Young Researcher Career Award from Umeå University for support of this work, and funding from MyFab for some of the sample preparation and characterization.

Received: July 16, 2015

Revised: November 4, 2015

Published online: January 27, 2016

- [1] S. Günes, H. Neugebauer, N. S. Sariciftci, *Chem. Rev.* **2007**, *107*, 1324.
- [2] A. J. Heeger, *Chem. Soc. Rev.* **2010**, *39*, 2354.
- [3] A. Facchetti, *Chem. Mater.* **2011**, *23*, 733.
- [4] S. R. Forrest, *Nature* **2004**, *428*, 911.
- [5] X. Yang, J. Loos, S. C. Veenstra, W. J. H. Verhees, M. M. Wienk, J. M. Kroon, M. A. J. Michels, R. A. J. Janssen, *Nano Lett.* **2005**, *5*, 579.
- [6] Y. Kim, S. Cook, S. M. Tuladhar, S. A. Choulis, J. Nelson, J. R. Durrant, D. D. C. Bradley, M. Giles, I. McCulloch, C.-S. Ha, M. Ree, *Nat. Mater.* **2006**, *5*, 197.
- [7] C. J. Brabec, S. Gowrisanker, J. J. M. Halls, D. Laird, S. Jia, S. P. Williams, *Adv. Mater.* **2010**, *22*, 3839.
- [8] H. Yang, T. J. Shin, L. Yang, K. Cho, C. Y. Ryu, Z. Bao, *Adv. Funct. Mater.* **2005**, *15*, 671.
- [9] M. Surin, P. Leclère, R. Lazzaroni, J. D. Yuen, G. Wang, D. Moses, A. J. Heeger, S. Cho, K. Lee, *J. Appl. Phys.* **2006**, *100*, 033712.
- [10] D. Gargi, R. J. Kline, D. M. DeLongchamp, D. A. Fischer, M. F. Toney, B. T. O'Connor, *J. Phys. Chem. C* **2013**, *117*, 17421.
- [11] S. Holliday, J. E. Donaghey, I. McCulloch, *Chem. Mater.* **2014**, *26*, 647.
- [12] P. D. Cunningham, L. M. Hayden, *J. Phys. Chem. C* **2008**, *112*, 7928.
- [13] R. Noriega, J. Rivnay, K. Vandewal, F. P. V. Koch, N. Stingelin, P. Smith, M. F. Toney, A. Salleo, *Nat. Mater.* **2013**, *12*, 1038.
- [14] A. Salleo, *Mater. Today* **2007**, *10*, 38.
- [15] R. J. Kline, M. D. McGehee, M. F. Toney, *Nat. Mater.* **2006**, *5*, 222.

- [16] A. Zen, J. Pflaum, S. Hirschmann, W. Zhuang, F. Jaiser, U. Asawapirom, J. P. Rabe, U. Scherf, D. Neher, *Adv. Funct. Mater.* **2004**, *14*, 757.
- [17] S. Hugger, R. Thomann, T. Heinzl, T. Thurn-Albrecht, *Colloid Pol. Sci.* **2004**, *282*, 932.
- [18] E. Verploegen, R. Mondal, C. J. Bettinger, S. Sok, M. F. Toney, Z. Bao, *Adv. Funct. Mater.* **2010**, *20*, 3519.
- [19] H. Siringhaus, P. J. Brown, R. H. Friend, M. M. Nielsen, K. Bechgaard, B. M. W. Langeveld-Voss, A. J. H. Spiering, R. A. J. Janssen, E. W. Meijer, P. Herwig, D. M. de Leeuw, *Nature* **1999**, *401*, 685.
- [20] R. J. Kline, M. D. McGehee, E. N. Kadnikova, J. Liu, J. M. J. Frechet, *Adv. Mater.* **2003**, *15*, 1519.
- [21] Y. Yang, K. Mielczarek, M. Aryal, A. Zakhidov, W. Hu, *Nanoscale* **2014**, *6*, 7576.
- [22] X. Lu, H. Hlaing, C.-Y. Nam, K. G. Yager, C. T. Black, B. M. Ocko, *Chem. Mater.* **2015**, *27*, 60.
- [23] Y. Yang, K. Mielczarek, M. Aryal, A. Zakhidov, W. Hu, *ACS Nano* **2012**, *6*, 2877.
- [24] E. Menard, M. A. Meitl, Y. Sun, J.-U. Park, D. J.-L. Shir, Y.-S. Nam, S. Jeon, J. A. Rogers, *Chem. Rev.* **2007**, *107*, 1117.
- [25] K. Trivedi, U. S. Bhansali, B. Gnade, W. Hu, *Nanotechnology* **2009**, *20*, 405204.
- [26] M. Fina, D. Liu, L. Ren, S. S. Mao, *Appl. Phys. A* **2011**, *105*, 323.
- [27] Y.-C. Lo, D. Li, Z. Sun, S. Shaik, X. Cheng, *J. Vac. Sci. Technol. B* **2012**, *30*, 06FB04.
- [28] S. Y. Oh, J.-Y. Lee, *Mol. Cryst. Liq. Cryst.* **2006**, *444*, 211.
- [29] H. Li, T. Chen, Y. Chao, *Nano Res.* **2014**, *7*, 938.
- [30] Y.-K. Wu, J.-H. Huang, W.-W. Tsai, Y.-P. Chen, S.-C. Lin, Y. Hsu, H.-W. Zan, H.-F. Meng, L. A. Wang, *IEEE Electron Device Lett.* **2013**, *34*, 313.
- [31] S.-H. Li, Z. Xu, G. Yang, L. Ma, Y. Yang, *Appl. Phys. Lett.* **2008**, *93*, 213301.
- [32] D. E. Johnston, K. G. Yager, H. Hlaing, X. Lu, B. M. Ocko, C. T. Black, *ACS Nano* **2014**, *8*, 243.
- [33] K. M. Coakley, B. S. Srinivasan, J. M. Ziebarth, C. Goh, Y. Liu, M. D. McGehee, *Adv. Funct. Mater.* **2005**, *15*, 1927.
- [34] M. D. McGehee, *MRS Bull.* **2009**, *34*, 95.
- [35] G. Wang, J. Swensen, D. Moses, A. J. Heeger, *J. Appl. Phys.* **2003**, *93*, 6137.
- [36] K.-J. Baeg, D. Khim, D.-Y. Kim, J. B. Koo, I.-K. You, W. S. Choi, Y.-Y. Noh, *Thin Solid Films* **2010**, *518*, 4024.
- [37] M. Aryal, K. Trivedi, W. Hu, *ACS Nano* **2009**, *3*, 3085.
- [38] J. A. Del Alamo, *Nature* **2011**, *479*, 317.
- [39] S. Y. Chou, P. R. Krauss, P. J. Renstrom, *J. Vac. Sci. Technol. B* **1996**, *14*, 4129.
- [40] L. J. Guo, *Adv. Mater.* **2007**, *19*, 495.
- [41] D. R. Barbero, M. S. M. Saifullah, P. Hoffmann, H. J. Mathieu, D. Anderson, G. A. C. Jones, M. E. Welland, U. Steiner, *Adv. Funct. Mater.* **2007**, *17*, 2419.
- [42] Z. Hu, M. Tian, B. Nysten, A. M. Jonas, *Nat. Mater.* **2009**, *8*, 62.
- [43] P. De Bruyn, A. H. P. van Rest, G. A. H. Wetzelaer, D. M. de Leeuw, P. W. M. Blom, *Phys. Rev. Lett.* **2013**, *111*, 186801.
- [44] G. A. H. Wetzelaer, P. W. M. Blom, *Phys. Rev. B* **2014**, *89*, 241201(R).
- [45] N. F. Mott, R. W. Gurney, *Electronic Process in Ionic Crystals*, Oxford University Press, Oxford **1940**.
- [46] C. F. Woellner, J. A. Freire, M. Guide, T.-Q. J. Nguyen, *J. Chem. Phys.* **2011**, *135*, 084108.
- [47] M. Brinkmann, *J. Polym. Sci. Pol. Phys.* **2011**, *49*, 1218.
- [48] Y.-K. Lan, C.-I. Huang, *J. Phys. Chem. B* **2009**, *113*, 14555.
- [49] D. H. Kim, Y. Jang, Y. D. Park, K. Cho, *J. Phys. Chem. B* **2006**, *110*, 15763.
- [50] H. Schulz, M. Wissen, N. Bogdanski, H.-C. Scheer, K. Mattes, C. Friedrich, *Microelectron. Eng.* **2006**, *83*, 259.
- [51] D. Jun, W. Zhengying, L. Shize, T. Yiping, *Microsyst. Technol.* **2013**, *19*, 1229.
- [52] Y. Xu, F. Tsumori, T. Toyooka, H. Kotera, H. Miura, *Jpn. J. Appl. Phys.* **2011**, *50*, 06GK11.
- [53] R. Khare, J. J. de Pablo, A. Yethiraj, *Macromolecules* **1996**, *29*, 7910.
- [54] R. H. Somani, B. S. Hsiao, A. Nogales, *Macromolecules* **2000**, *33*, 9385.
- [55] J. E. Northrup, *Phys. Rev. B* **2007**, *76*, 245202.
- [56] C. Luo, A. K. K. Kyaw, L. A. Perez, S. Patel, M. Wang, B. Grimm, G. C. Bazan, E. J. Kramer, A. J. Heeger, *Nano Lett.* **2014**, *14*, 2764.
- [57] B. T. O'Connor, O. G. Reid, X. Zhang, R. J. Kline, L. J. Richter, D. J. Gundlach, D. M. DeLongchamp, M. F. Toney, N. Kopidakis, G. Rumbles, *Adv. Funct. Mater.* **2014**, *14*, 3422.